論文 / 著書情報
Article / Book Information

Title	FORENSIC ANALYSIS OF REINFORCED CONCRETE HALF-JOINTS USING NONLINEAR FINITE ELEMENT ANALYSIS
Authors	Nobuhiro Chijiwa, Benny Suryanto, Ryota Kurihara
Citation	Advances in Construction Materials, Proceedings of the ConMat'20, 7-3_4, ,
Pub. date	2020, 9

FORENSIC ANALYSIS OF REINFORCED CONCRETE HALF-JOINTS USING NONLINEAR FINITE ELEMENT ANALYSIS

Nobuhiro Chijiwa[1], Benny Suryanto[2], and Ryota Kurihara[3]

[1] Associate Professor, Tokyo Institute of Technology, chijiwa@cv.titech.ac.jp
[2] Associate Professor, Heriot-Watt University, b.suryanto@hw.ac.uk
[3] PhD student, Tokyo Institute of Technology, kurihara.r.aa@m.titech.ac.jp

ABSTRACT

Half-joint construction has gained its global popularity due to its simple design and construction processes. Many half-joint bridges have been built around the world since decades ago and the majority are currently undergoing severe deterioration problems. Unfortunately, this type of bridge construction is amongst the hardest to inspect, particularly in the joint region where concrete deterioration and corrosion of the steel reinforcement are common. The situation is exacerbated by the fact that a significant percentage of the bridges is now approaching its service life and hence requires special attention. However, the assessment of the remaining performance of a half-joint presents significant engineering challenges, not only due to the complexities of the deterioration levels, but also because of the presence of non-compliant reinforcement detailing.

In this paper, nonlinear finite element analysis is used to investigate the load capacity and failure mode of a series of full-scale bridge half-joints recently tested in the UK. The analysis platform employed implements nonlinear constitutive models of concrete which are formulated based on the smeared multi-directional fixed-crack approach. The analysis results show that there is a good agreement between the numerical and experimental data presented in terms of load-deflection response, load capacity, mode of failure and crack patterns at failure. Insights into the combined influence of non-compliant reinforcement detailing and corrosion of reinforcement on load capacity, overall stiffness and failure mode are presented. Overall this paper supports the conviction that nonlinear finite element analysis provides a powerful tool for forensic assessment of deteriorated reinforced concrete structures.

Keywords: Finite Element, Half-joint, Reinforced Concrete, Corrosion, Deterioration, Assessment.

Nobuhiro Chijiwa, DEng
Tokyo Institute of Technology
2-12-1-M1-1, Ookayama
Meguro, Tokyo 152 8552
Japan

Email: chijiwa@cv.titech.ac.jp
Tel: +81-3-5734-3767

1. INTRODUCTION

Half-joint, also referred to as dapped-end in some regions, was introduced into bridge construction in order to simplify design and construction processes. Generally, half-joint bridges have multiple (typically three) spans, with the half-joints being used normally over the central suspended span (see, for example, Figure 1(a)). The term half-joint was introduced following the joint geometry which comprises a pair of inverted corbels that protrude from the end of a structural element (commonly referred to as a nib) at a distance of approximately half of the overall depth of the girder and hence the name half-joint. This joint configuration is common in Gerber bridge construction as it enables bridge girder over the suspended span to be constructed off-site, which not only helps to reduce construction time and cost, but also improve quality. Owing to these advantages, half-joint has since gained its global popularity in bridge construction around the world [1]. In Scotland alone, for example, a total of 39 half-joint bridges and 12 other footbridges have been constructed over the past five decades [2], giving the national transport agency a total of 275 half-joints to inspect and repair on a regular basis.

Whilst half-joint construction is attractive in terms of structural design and construction, the joint geometry adds significant difficulty to inspection and maintenance. More specifically, due to the nature of the joint configuration, the concrete inside the L-shaped joint is no longer accessible, making half-joint bridges amongst the hardest to inspect. Furthermore, in the event of expansion joint failure, the joint becomes vulnerable to deterioration. During a winter season, for example, deicing salts can get through the joint and accumulate. Over a long term, this can lead to corrosion of the steel reinforcement [3-5] and loss of steel section which reduces the safety margins. Other influencing factors include concrete degradation [6], vehicle impact [7] and non-compliant detailing [1, 6]. Given the vulnerability of half-joints to deterioration, it is not surprising that many of half-joint bridges are now undergoing severe deterioration problems, with some even experiencing catastrophic failure. Figure 1(b) displays the condition of one of the half-joints of the de la Concorde overpass in Quebec (Canada) in 2006 [8] and another joint of the Annone overpass in Lecco (Italy) in 2016 [7]. Severe cracking was clearly evident prior to their catastrophic failure. In the case of the de la Concorde overpass, this appears to originate from the end of the full depth section, whereas in the Annone overpass, it appears to originate from the re-entrant corner. These two major incidents have shown that the assessment of the remaining performance of half-joints is difficult as it is not only affected by the as-built details which would influence the mode of failure, but also affected by the extent of deterioration.

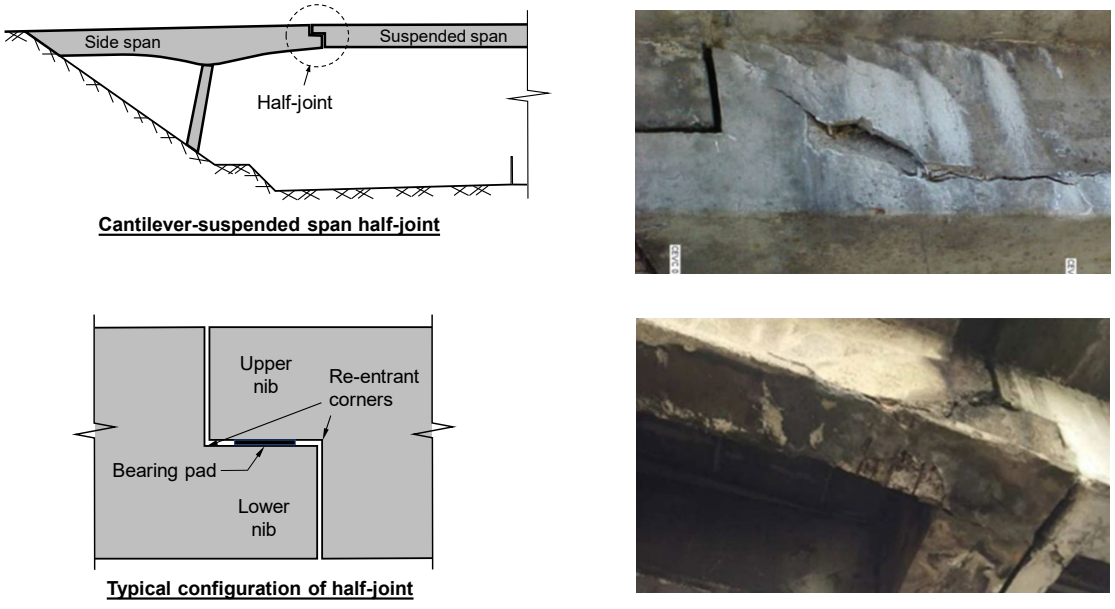

Figure 1. (a) Schematic of a half-joint bridge and close-up of a half-joint. (b) conditions of the half-joint of the de la Concorde overpass in Quebec [8] (top) and of the Annone overpass in Lecco (bottom) [7] prior to failure.

In this paper, nonlinear finite element analysis is used to investigate the load capacity and failure mode of a series of full-scale half-joints tested recently at the University of Cambridge in the UK [1] in which the influence of non-compliant detailing was specifically studied. This paper aims to provide an improved understanding of the mechanisms underlying the response observed experimentally at the structural level. The results of these full-scale experiments are used to validate numerical FE models, which were further used to investigate of the influence of steel corrosion on structural performance thereby extending the scope of the original experimental investigation.

2. FINITE ELEMENT MODELLING

2.1. Beam geometry and test parameters

Figure 2(a) displays the longitudinal profile and bar configuration of four half-joints simulated in this paper. All half-joints had an overall width of 400 mm and depth of 700 mm, which was reduced to 325 mm at the nib. The first half-joint had 4 diagonal bars of 12 mm diameter and 3 U-bars of the same diameter (labelled NS-REF); the second beam had the U-bars removed (labelled NS-NU); the third beam had the diagonal bars removed (NS-ND); and the last beam had a reduced number of shear links (NS-RS). Unless otherwise stated, other reinforcement in NS-NU, NS-ND and NS-RS half-joints was identical to the reference beam (NS-REF).

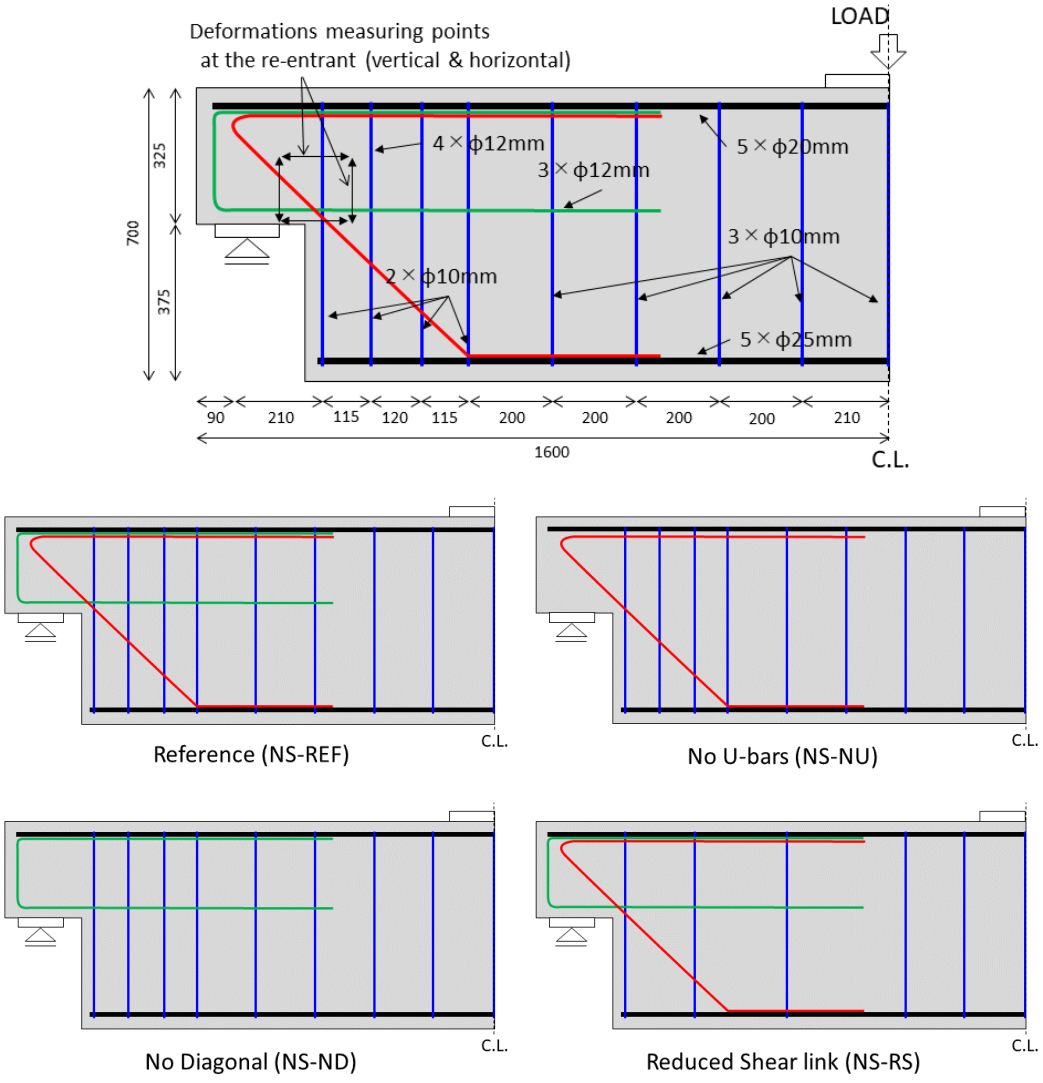

Figure 2. Reinforcement details for the four half-joints tested at the University of Cambridge [1].

Apart from diagonal and U-bars, the half-joints were reinforced with 5 longitudinal tension bars of 25 mm diameter and 5 longitudinal compression bars of 20 mm diameter. Four two-legged shear links of 10 mm diameter were provided over the region next to the nib at a spacing of 115 mm, whereas deeper into the beam, the spacing of the shear links was increased to 200 mm, but with one additional leg provided. Two different test configurations were incorporated in the experiment. In the initial configuration, the half-joint was supported on both nibs at a distance of 3100 mm and then loaded. Once the weaker half-joint reached its ultimate limit, the support at the failed end was moved inwards into the full depth section and loading was then resumed until failure of the other (stronger) end.

2.2. Finite element meshes and analysis platform

Nonlinear finite element analysis was undertaken using the software package developed at the University of Tokyo, COM3 [9]. It employs nonlinear constitutive models of concrete which are implemented within the multi-directional fixed-crack approach (see, for example, Fig. 3(b)). Using this analysis platform, the 3D behaviour of cracked concrete under general loading conditions can be well simulated, including crack-to-crack interactions in reinforced concrete beams under complex loading conditions [10], long-term deflection of long-span prestressed concrete bridges [11] and distressed structures (i.e. due to corrosion of steel reinforcement) under seismic loading [12].

In this study, the half-joint beams were modelled using a mesh of some 3000 cubical reinforced concrete elements (see Fig. 3(a)). Due to symmetry, only half of the beams was modelled in this initial study. The reinforcement in both longitudinal (x) and transverse (z) directions was provided in a smeared manner, with the centroids of each smeared area aligned with the centroids of the actual steel. Figure 3(a) displays an example of the reinforcement ratio inputted for NS-REF specimen. In an element with different types of steel reinforcement present, the total reinforcement ratio was inputted (the orange and red areas in Fig. 3(a)). The support and loading plates were modelled using the available steel element.

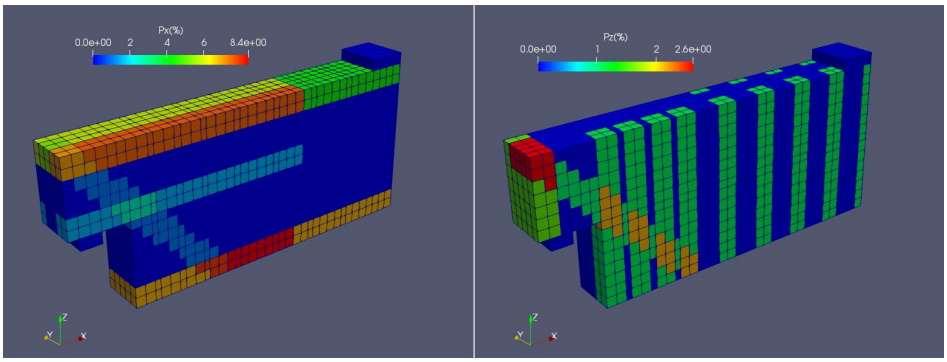

(a) Finite element mesh showing overall geometry and steel reinforcement ratio (left: ρ_x (%) and right: ρ_z (%)).

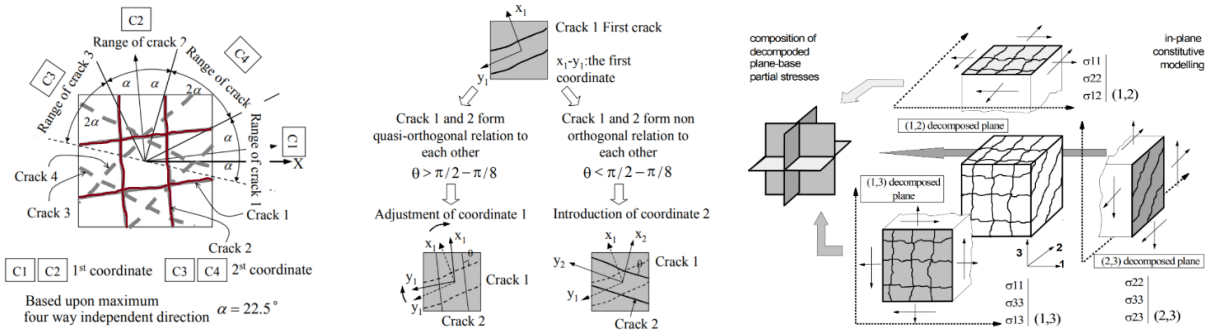

(b) Multi-directional fixed-crack approach [9].

Figure 3. Finite element mesh and crack modelling in the analysis.

The concrete and reinforcement material properties used in the analysis were as reported in the original publication, except for the tensile strength of concrete which was estimated from the compressive strength (= 36.8 MPa). In this study, the tensile strength of the concrete was taken as 2.54 MPa to consider initial shrinkage-induced stresses. The yield and rupture strengths of the steel reinforcement were also set as reported (see Table 1). The ultimate strain of the steel was taken as 0.09 (assumed value) to consider the fact that the reinforcement in the UK is generally less ductile than those normally used in seismic prone countries such as Japan. Both the 10 mm and 12 mm bars used in the experiment were cold-formed bars and, as such, strain hardening in the analysis was assumed to start immediately when the bar reached the yield strength. It was noted that the 25 mm bars were hot-rolled bars and hence a stress-strain response with a proper yield plateau was considered.

Table 1. Material properties for the steel reinforcement

Bar size [mm]	f_y [MPa]	f_t [MPa]	E_s [MPa]	ε_{sh} [mm/mm]	ε_{rp} [mm/mm]	Remark
10	539	596	200	0.00270	0.09#	Cold deformed
12	529	559	200	0.00265	0.09#	Cold deformed
20	578&	674&	200&	0.02890&	0.09&	Hot rolled
25	578	674	200	0.02890	0.09	Hot rolled

Note: # assumed property. & similar value to 25 mm bar (assumed).

2.3. Modelling of steel corrosion

The corrosion model of Toongoenthong-Maekawa [13] was used to simulate the corrosion of steel in the half-joint beams and associated corrosion-induced cracking. Using this model, it is possible to consider the expansion of corrosion products into the surrounding concrete (and the corresponding lateral pressure), steel section loss, and concrete cracking. A linear relationship is considered between the amount of mass loss (and associated corrosion product) and induced tensile stresses in the surrounding concrete, as shown in the schematic in Figure 4.

When the corrosion product reaches the critical amount, cracking forming around the steel is asssumed to have reached the concrete surface [13]. At this point, corrosion gel/product can be discharged and the linearity is, therefore, lost. As a result, although corrosion process still continues (hence the mass loss and the amount of corrosion product), it can be expected that the lateral pressure induced by the expansion of the corrosion product will hardly increase due to stress relaxation resulting from the cracking[14]. To this end, it is assumed that the corrosion induced stress becomes constant when the mass loss of the steel reaches a critical amount, following the recommendation by Biswas and co-workers [15]. This limit is referred to as the crack generation limit, CGL, and can be calculated from:

$$CGL = A_{st} W_{cr} \gamma_{st} \tag{1}$$

where A_{st} is the cross-sectional area of rebar, W_{cr} is the critical corrosion amount (%) and γ_{st} is the unit weight of the steel bar. The critical corrosion amount can be approximated from:

$$W_{cr} = a\, c^{2.07} \tag{2}$$

where a is a constant and be taken as 0.0018 for the corrosion amount to cause cracking of reinforced concrete[16], and c is the cover thickness (mm).

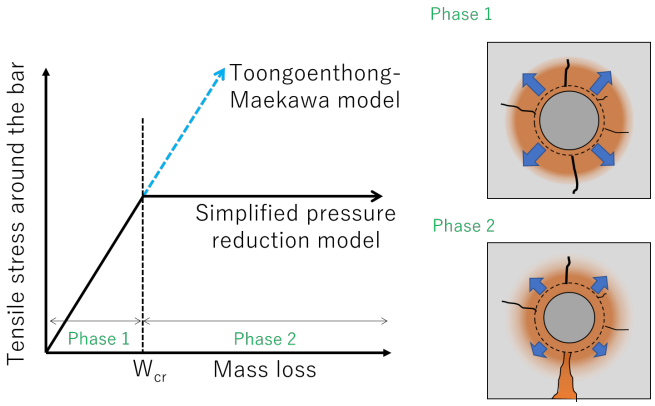

Figure 4. Relationship between mass loss of the rebar and corrosion induced tensile stresses [14].

In addition to crack formation and section loss, it is recognised that corrosion may alter the bond between the concrete and the steel, and this in turn can influence the distribution of cracking under loading. This bond alteration can be reflected in the tension stiffening paramater which is normally taken as 0.4 when there is a well-distributed of crack formation around the steel. When there is a large reduction in steel cross-section, this may result in local bond reduction and hence non-uniform crack distribution. In this study, the tension stiffening parameter was taken simply as equal to plain concrete (2.0) when the critical corrosion amount is greater than 0.01 mg/mm^2.

3. SIMULATION RESULTS AND DISCUSSIONS

3.1. Summary of experimental findings

According to the PCI handbook [17], there are five common modes of failure in half-joint: (I) flexural failure of the nib; (II) direct vertical shear between the nib and full-depth portion; (III) diagonal tensile failure initiated from the re-entrant corner; (IV) diagonal tensile failure in the nib; (V) diagonal tensile failure in the full-depth portion. It is reported in [1] that both reference (NS-REF) and no diagonal bars (NS-ND) specimens experienced type III failure, with NS-ND exhibiting a more localised failure at the re-entrant corner. The removal of U-bars (NS-NU) was found to increase the inclination of the failure cracks at the re-entrant corner to a nearly vertical. It was also found that the reduction in the amount of shear links (NS-RS) caused the failure crack to form at the full-depth section and hence type V failure.

3.2. Effect of reinforcement arrangement

The load-deflection responses obtained from the nonlinear finite element analysis are compared to experimental data in Figure 5, with comparisons of failure crack patterns and predicted principal strain plots presented in Figure 6 and comparisons of load-deformation responses at the re-entrant corner in Figure 7. In general terms, reasonably accurate predictions of load-deflection response, load capacity, mode of failure, crack patterns and location of failure are obtained. With reference to Figures 5, it is evident that the trend of the load capacity of the four half-joints can be well simulated, although the post-cracking stiffness and accordingly the beam deflection at peak load are overestimated. This is due to the fact that in the experiment, one of the supports was moved inwards into the end of the full-depth section once the weaker joint had reached their ultimate capacity. This support movement has not been considered in this initial study as the exact pair of half-joints in each beam was not reported in [1]. However, it is anticipated that this would not significantly alter the internal mechanism of force transfer at the other (stronger) end and hence the accuracy of the predictions. This warrants further investigation and will be the direction of our future work.

Comparisons of the failure crack patterns with the principal strain fields are presented in Figure 6. As in experiment, it is shown that the propagation of diagonal cracking at the re-entrant corner is altered by the removal of U-bars (NS-NU) due to the loss of horizontal confinement. When the diagonal bars

(NS-ND) is removed, the diagonal crack is more localised at the re-entrant corner and in good agreement with the observed crack pattern. The reduction in shear links (NS-RS) is predicted to move the failure crack into the full-depth portion which agrees well with test evidence. Figure 6 compares the predicted and observed deformation at the re-entrant corner and the trend is well reproduced in the analysis.

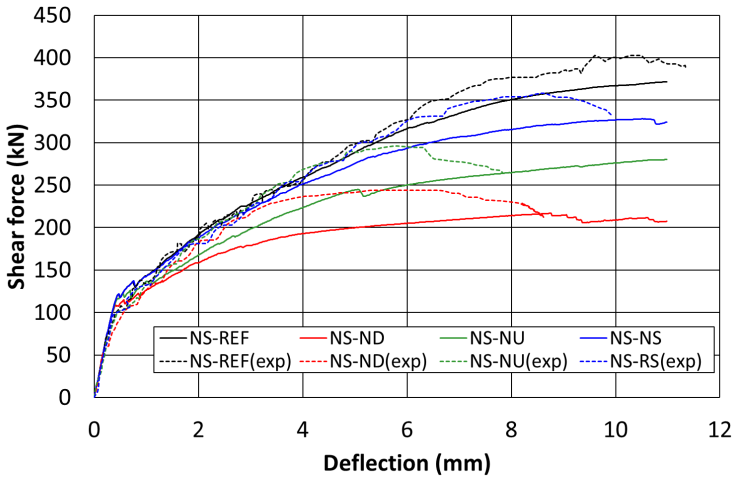

Figure 5. Predicted and observed [1] load-deflection responses.

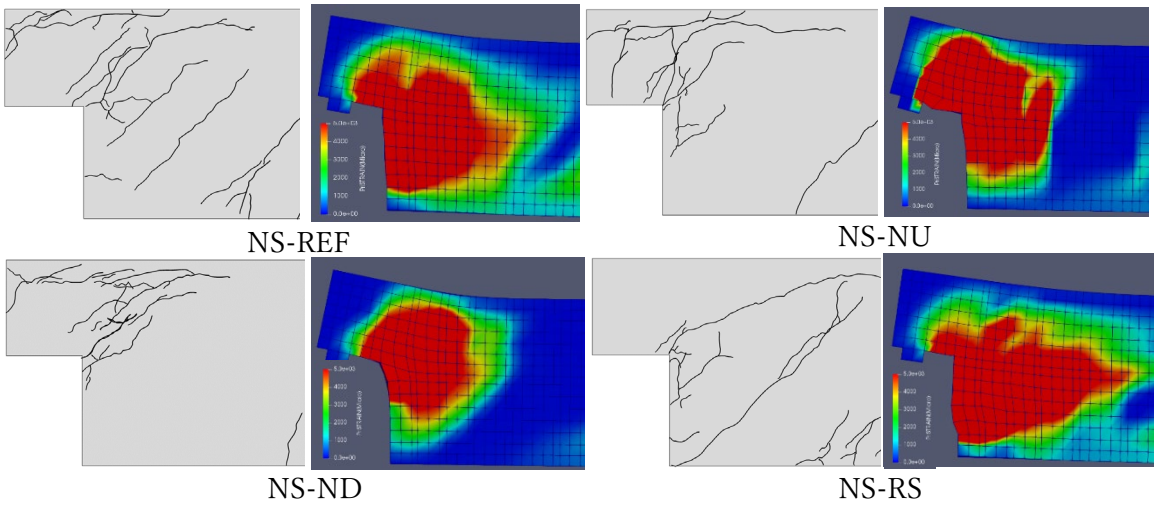

Figure 6. Crack patterns at failure [1] vs principal strain fields obtained from the FE analysis.

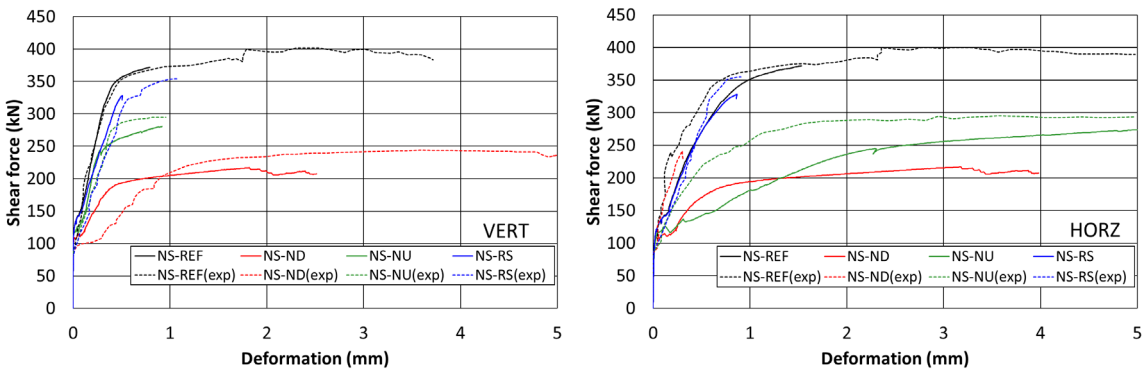

Figure 7. Comparison of load-deformation response (left: vertical, right: horizontal).

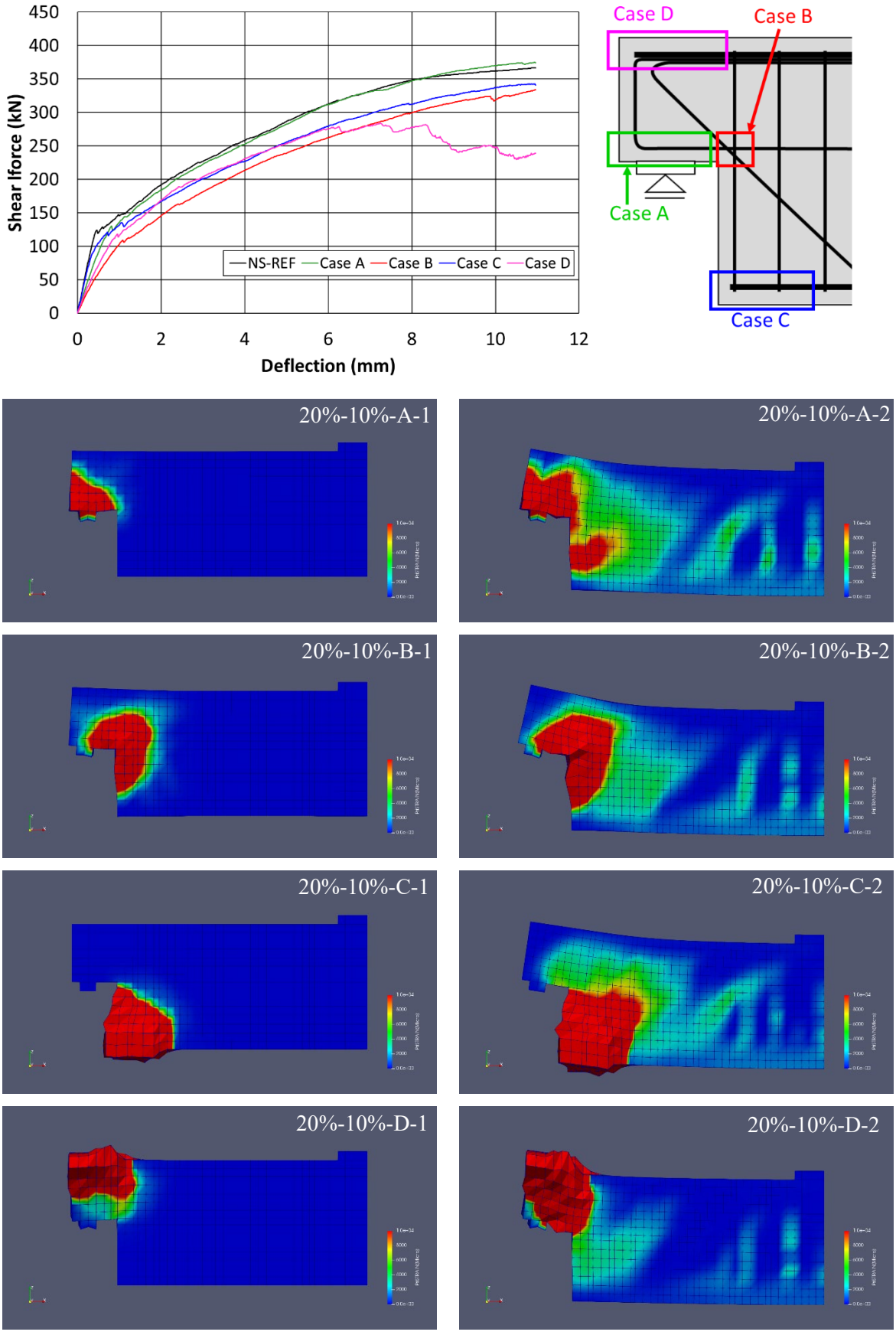

Figure 8. Predicted load-deflection responses and principal strain distributions assuming a mass loss of 20%, with a critical corrosion amount (corrosion gel/product discharge) taken as 10%.

3.3. Effect of corrosion of steel reinforcement

Parametric analysis was undertaken to investigate the influence of the extent and location of steel corrosion on structural response. Four case studies were considered (see Fig. 8): Case A, with the corrosion applied to the U-bars on the lower part of the nib; Case B applied to all (diagonal, U and one link) bars at the re-entrant corner; Case C applied to the bars at the lower part of the full-depth section; and Case D applied to the U-bars at the upper part of the nib (or opposite to Case A). In all cases, the corrosion was first introduced onto the beam assuming a mass loss of 20%, with the critical corrosion amount taken as 10%. The half-joint beam was then loaded to failure as in the experiment.

Figure 8 displays the predicted load vs deflection response of the beam, together with the predicted principal strain plots during the initial (corrosion) stage and at failure. The first number shown in the corresponds to the amount of mass loss (i.e. 20%), the second number (i.e. 10%) corresponds to the critical corrosion amount when the lateral pressure is assumed to be constant, the letter represents the Corrosion Case (i.e. A/B/C/D), and the number at the back corresponds to analysis stage (1: initial/corrosion stage; 2: loading stage). It is evident from the Figure 8 Case D (corrosion of U-bars on the upper part of the nib) exhibits the most significant reduction in load capacity and overall ductility, whereas Case B (corrosion at the re-entrant corner) displays the largest reduction in initial stiffness apart from a reduction in load capacity indicating that corrosion in these two locations will influence behaviours under both serviceability and ultimate limit state. It is worth noting that Case D has not been considered in the original experimental study as corrosion of bars in this case might have well hidden under the asphalt layer and, therefore, not identified during the site visual inspection. Corrosion at location A (U-bars at the lower part of the nib) is shown to only influence the initial stiffness and has little effect on the overall capacity. This could be attributed to the fact the half-joint tested relies more on the diagonal bars at the re-entrant corner which in this case remain fully intact (no corrosion). Similarly, corrosion at location C (longitudinal bars at the bottom of the full-depth section) is shown to exert a minimal influence, although it has the potential to shift the critical area from the re-entrant corner (as in the original or other corrosion cases) to the full-depth section of the beam highlighting the increasing importance of the shear links once the bottom bars are corroded. Furthermore, it is interesting to note that Case A exhibits somewhat different failure crack pattern that NS-NU half-joint displayed earlier in Figure 7, indicating the need for accurate representation of damage (i.e. corrosion induced cracking; hence crack-to-crack interactions) than a simple removal of U-bars as in the original experiment.

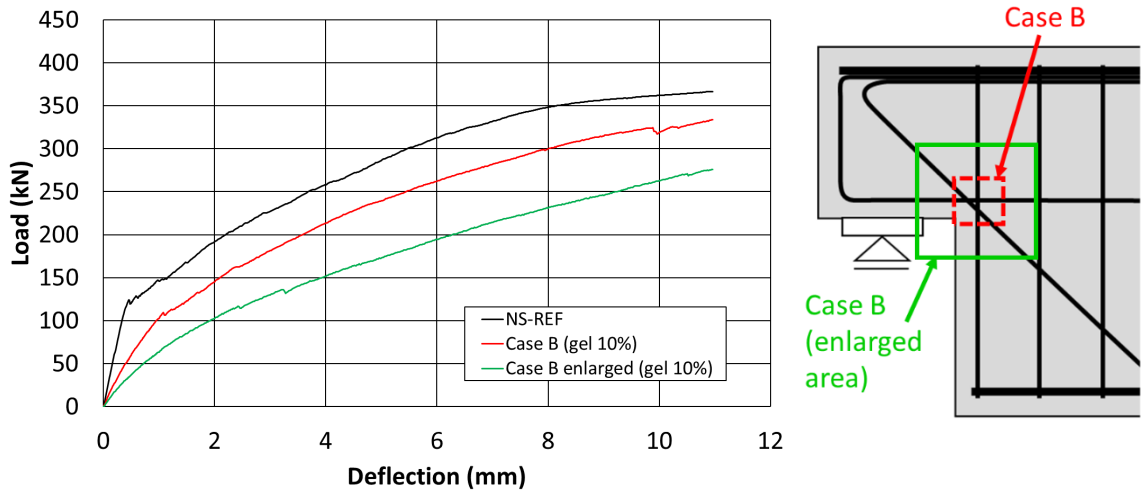

Figure 9. Predicted load-deflection responses with original and enlarged areas of corrosion at the re-entrant corner (Case B).

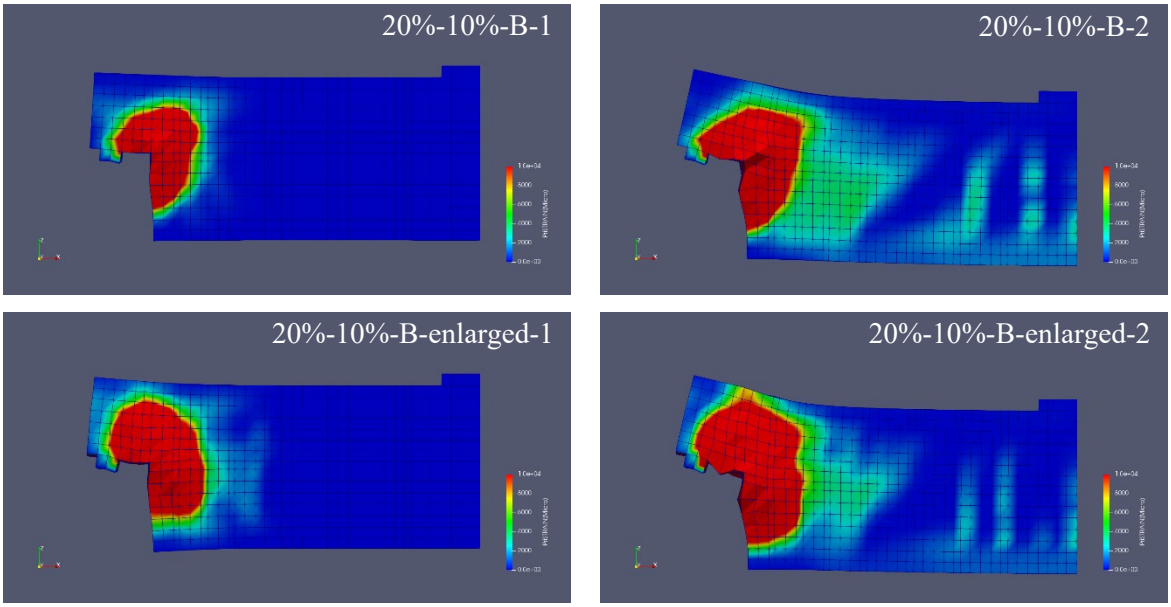

Figure 10. Predicted principal strain plots with original and enlarged areas of corrosion at the re-entrant corner (Case B).

Based on the above findings, a further parametric analysis was undertaken to investigate the influence of area of corrosion at the re-entrant corner (Case B) on the response of the half-joint. The same corrosion level was applied as before (i.e. 20% mass loss with a gel discharge at 10%). Figure 9 presents the predicted load-deflection response, with the principal strain plots presented in Figure 10. It is apparent from Figure 9 that the increase in area of corrosion results in a more dramatic reduction in load capacity and overall stiffness. This may be attributed to the fact that the initial damage induced by the corrosion (initial cracking) alters the internal mechanism of stress transfer (i.e. path of diagonal strut and tie in the concrete). This finding provides an exciting scope of further investigation and work is continuing in this respect.

4. CONCLUDING REMARKS

Nonlinear finite element analyses were undertaken to simulate the structural response of a series of half-joints which contain non-compliant reinforcement detailing. The challenge was to accurately capture the role of different reinforcement on overall structural response. It is shown that the numerical platform employed can be used to accurately determine the anticipated load-deflection response, load capacity, mode of failure and crack patterns at failure. From the analysis of the original series of the half-joint beams, it is also shown that it is the steel reinforcement at the re-entrant corner (particularly the diagonal bars) that has a significant influence on load capacity and the response at the ultimate limit state.

Parametric studies were undertaken to further investigate the influence of corrosion of steel reinforcement at critical locations on overall structural responses. Key parameters include four possible locations of corrosion (upper and lower parts of nib, re-entrant corner, lower part of the full-depth section). A constant mass loss of 20% was considered, with a limit on lateral pressure induced corrosion. Of these analysis cases, it is shown that corrosion of bars at the re-entrant corner and the upper part of the nib have a considerable influence on overall load-deflection responses, particularly on load capacity and member stiffness. It is also shown that the reduction in load capacity and member stiffness is not only affected by the location of corrosion, but also influenced by the area of corrosion. The importance of proper consideration of initial damage in the concrete (i.e. corrosion induced cracking) is

demonstrated as in some cases it is shown that the influence of corrosion cannot be achieved by a simple removal of steel reinforcement.

REFERENCES

[1] Desnerck, P., Lees, J. M., & Morley, C. T. (2016). Impact of the reinforcement layout on the load capacity of reinforced concrete half-joints. *Engineering Structures*, 127, 227-239.

[2] Transport Scotland (2006). TS Interim Amendment No. 20-Concrete half-joint deck structures.

[3] O'Connor, K., Wynd, B., Cunningham, G., & MacPherson, D. (2019, December). Maintenance of early reinforced-concrete road bridges in Aberdeenshire, Scotland. In: *Proc. the Institution of Civil Engineers-Bridge Engineering* (Vol. 172, No. 4, pp. 293-302). Thomas Telford Ltd.

[4] Kim, J., McCarter, W. J., Suryanto, B., Nanukuttan, S., Basheer, P. M., & Chrisp, T. M. (2016). Chloride ingress into marine exposed concrete: A comparison of empirical-and physically-based models. *Cement and Concrete Composites*, 72, 133-145.

[5] Kim, J., McCarter, W. J., & Suryanto, B. (2018). Performance assessment of reinforced concrete after long-term exposure to a marine environment. *Construction and Building Materials*, 192, 569-583.

[6] Mitchell, D., Marchand, J., Croteau, P., & Cook, W. D. (2011). Concorde overpass collapse: structural aspects. *Journal of performance of constructed facilities*, 25(6), 545-553.

[7] Di Prisco, M., Colombo, M., Martinelli, P., & Coronelli, D. (2018). The technical causes of the collapse of Annone overpass on SS. 36. In: *Proc. Italian Concrete Days 2018* (pp. 1-16). Lecco, Italy.

[8] Johnson, P. M., Couture, A., & Nicolet, R. (2007). *Report of the Commission of inquiry into the collapse of a portion of the de la Concorde overpass*. Government of Quebec.

[9] Maekawa, K., Okamura, H. & Pimanmas A. 2003. *Nonlinear mechanics of Reinforced Concrete*. London, Spon Press.

[10] Gebreyouhannes, E., Chijiwa, N., Fujiyama, C., & Maekawa, K. (2008). Shear fatigue simulation of RC beams subjected to fixed pulsating and moving loads. *Journal of Advanced Concrete Technology*, 6(1), 215-226.

[11] Ohno, M., Chijiwa, N., Suryanto, B., & Maekawa, K. (2012). An investigation into the long-term excessive deflection of PC viaducts by using 3D multi-scale integrated analysis. *Journal of advanced concrete technology*, 10(2), 47-58.

[12] Chijiwa, N., & Maekawa, K. (2015). Thermo-hygral case-study on full scale RC building under corrosive environment and seismic actions. *Journal of Advanced Concrete Technology*, 13(10), 465-478.

[13] Toongoenthong, K., & Maekawa, K. (2005). Simulation of coupled corrosive product formation, migration into crack and propagation in reinforced concrete sections. *Journal of Advanced Concrete Technology*, 3(2), 253-265.

[14] Gebreyouhannes, E., & Maekawa, K. (2016). Nonlinear gel migration in cracked concrete and broken symmetry of corrosion profiles. *Journal of Advanced Concrete Technology*, 14(6), 271-286.

[15] Biswas, R. K., Iwanami, M., Chijiwa, N., & Uno, K. (2020). Effect of non-uniform rebar corrosion on structural performance of RC structures: A numerical and experimental investigation. *Construction and Building Materials*, 230, 116908.

[16] Oh, B.H., Kim, K.H., & Jang, B.S. (2009). Critical corrosion amount to cause cracking of reinforced concrete structures, *ACI Material Journal*. 106, 333–339.

[17] Prestressed Concrete Institute. (2017). PCI Design Handbook: precast and prestressed concrete.